Nano Today 48 (2023) 101730

Contents lists available at ScienceDirect

Nano Today

journal homepage: www.elsevier.com/locate/nanotoday

A highly efficient needle-free-injection delivery system for mRNA-LNP vaccination against SARS-CoV-2

Shanhong Mao [a,e,*,1], Shiyou Li [b,1], Yuxin Zhang [c,1], Luoxin Long [a], Junfeng Peng [b], Yuanyan Cao [a], Jessica Z. Mao [f], Xin Qi [c], Qi Xin [b], Guoliang San [c], Jing Ding [c], Jun Jiang [b], Xuejiao Bai [b], Qianting Wang [b], Pengfei Xu [b], Huan Xia [b], Lijun Lu [b], Liangzhi Xie [d], Desheng Kong [d], Shuangli Zhu [g], Wenbo Xu [g]

[a] School of Biomedical Engineering, Capital Medical University, Beijing 100069, China
[b] Tricision Biotherapeutic Inc, Beijing 100176, Zhuhai 519040, China
[c] Beijing QS Medical Technology Co.,Ltd., Beijing 100176, China
[d] Beijing Engineering Research Center of Protein and Antibody, Sinocelltech Ltd., Beijing 100176, China
[e] School of Light Industry, Beijing Technology and Business University, Beijing 100048, China
[f] School of Veterinary Medicine & Biomedical Sciences, Texas A&M, College Station, TX 77843, USA
[g] National Institute for Viral Disease Control and Prevention, Chinese Center for Disease Control and Prevention, Beijing 102206, China

ARTICLE INFO

Article history:
Received 15 November 2022
Received in revised form 5 December 2022
Accepted 13 December 2022
Available online 21 December 2022

Keywords:
SARS-CoV-2
Needle-free injection (NFI)
Needle injection (NI)
Lipid Nanoparticle (LNP)
mRNA vaccine

ABSTRACT

Despite the various vaccines that have been developed to combat the coronavirus disease 2019 (COVID-19) pandemic, the persistent and unpredictable mutations of the severe acute respiratory syndrome coronavirus 2 (SARS-CoV-2) require innovative and unremitting solutions to cope with the resultant immune evasion and establish a sustainable immune barrier. Here we introduce a vaccine-delivery system with a combination of a needle-free injection (NFI) device and a SARS-CoV-2-Spike-specific mRNA-Lipid Nanoparticle (LNP) vaccine. The benefits are duller pain and a significant increase of immunogenicity compared to the canonical needle injection (NI). From physicochemical and bioactivity analyses, the structure of the mRNA-LNP maintains stability upon NFI, contradictory to the belief that LNPs are inclined towards destruction under the high-pressure conditions of NFI. Moreover, mRNA-LNP vaccine delivered by NFI induces significantly more binding and neutralizing antibodies against SARS-CoV-2 variants than the same vaccine delivered by NI. Heterogeneous vaccination of BA.5-LNP vaccine with NFI enhanced the generation of neutralizing antibodies against Omicron BA.5 variants in rabbits previously vaccinated with non-BA.5-specific mRNA-LNP or other COVID-19 vaccines. NFI parameters can be adjusted to deliver mRNA-LNP subcutaneously or intramuscularly. Taken together, our results suggest that NFI-based mRNA-LNP vaccination is an effective substitute for the traditional NI-based mRNA-LNP vaccination.

Introduction

Inducing herd immunity through mRNA vaccines has been demonstrated to be a highly effective strategy for preventing the spread of SARS-CoV-2 [1]. However, the mutations in the spike (S) protein of SARS-CoV-2 that confer immune escape from neutralizing antibodies have weakened the immune barrier established by current available vaccines, including mRNA, inactivated, and recombinant protein vaccines [2–7]. Researchers expect that heterologous-booster injections of existing vaccines will become a strategy to provide human beings a high antibody level to combat the variants of concern (VOCs) [8–10]. Among these vaccines, the mRNA type was used for large scale vaccinations due to its proven safety, strong immunogenicity, and short research-development-production cycle [11]. The US Food and Drug Administration (FDA) and the European Medicines Agency (EMA) granted emergency use authorization of Moderna and Pfizer/BioNTech bivalent COVID-19 mRNA vaccine boosters targeting Omicron BA.4/BA.5, which were approved to enhance protection for vulnerable population groups, such as elders, children, and immunodeficient or immunocompromised individuals [12–14]. To date, the administration

* Corresponding author at: School of Biomedical Engineering, Capital Medical University, Beijing 100069, China.
E-mail address: maosh@ccmu.edu.cn (S. Mao).
[1] These authors contribute equally to this work.

https://doi.org/10.1016/j.nantod.2022.101730

of mRNA vaccine boosters can only be done via trained professionals using conventional syringes. Vaccine hesitancy caused by needle phobia and the scarcity of trained professionals are two major issues facing high-risk populations when receiving vaccinations [15]. To make the vaccination program more efficient and accessible, alternative vaccine delivery methods are needed.

Needle-free injection (NFI) technology uses a high-pressure source to promote formation of high-speed liquid jets that penetrate the epidermal and dermal layers and deliver drugs into the subcutaneous or intramuscular layer [16]. Compared to the traditional injection method (NI) that uses a needle to penetrate skin layers and deliver a bulk of liquid that is gradually absorbed, NFI delivers medicines in a more dispersed form with a significant increase of contact area between injected liquid and capillaries, thus facilitating drug absorption and reducing the pain of inoculation [17]. As for vaccine delivery and utilization, the skin and subcutis have a complex immune system that is histologically represented by skin-associated lymphoid tissue (SALT), which is composed of dendritic cells (DCs), mast cells, B and T lymphocytes, and keratinocytes [18]. This immunologically complex organ has the ability to respond to infectious and noninfectious aggressive agents through innate and adaptive immunity mechanisms, which are called barrier epithelium immune responses [19]. In recent years, the application of NFI technology has been explored for use in many medical functions, such as vaccination, insulin injections, and medical cosmetology [20–22]. NFI-deliveries via both intradermal and intramuscular injections have been used for different types of vaccines, including inactivated polio vaccine (IPV) [23], influenza vaccine [24], hepatitis B vaccine [25], human papillomavirus vaccine (HPV) [26], and diphtheria pertussis tetanus (DPT) vaccine [27]. Yet, exploration of the utilization of NFI with Covid-19 vaccines, especially mRNA type vaccines, remains to be conducted.

In this study, we develop a novel integrated system of LNP-based COVID-19 mRNA vaccines with NFI devices, and study the stability of mRNA-LNP particles under the high-pressure conditions imposed by the NFI system. Furthermore, using both rat and rabbit animal models, we elucidate the system's unique capability of generating a high level of antibodies and its high effectiveness against Omicron sublineages. We also provide insight into the future application of NFI technology on mRNA type therapies.

Materials and methods

NFI-based dispersive depth-exploration of contents in animal models

Rats (5–7 weeks) and rabbits (4–6 months) were injected in the lateral thigh area with an mRNA-LNP vaccine containing methylene blue as indicator, using QS-P NFI-devices (Quinovare, China). The NFI spring forces adopted in this test were 200 N, 220 N, 240 N, 260 N, 280 N for rats and 280 N, 300 N, 320 N, 340 N, 365 N for rabbits, respectively. Each panel of spring force tests contained at least 4 animals. The injection site was dissected immediately after NFI-delivery to observe the coverage, depth, and diffusion of the methylene blue. All use of study animals was approved by the Institutional Animal Care and Use Committee.

Determination of flow velocity

The velocity of the liquid jet was examined by measurement and confirmed using a theoretical formula. First, the measured motor position (the control variable) was used to calculate piston speed, which is related to the volumetric average jet speed by

$$v_j = \frac{v_p \cdot A_p}{A_o}$$

where v_j is the jet speed, v_p is the speed of the piston, A_p is the area of the piston and A_o is the area of the nozzle orifice. This measurement assumed that the piston speed and volume flow rate were proportionally related, which was true for the vast majority of injections.

The calculated velocities were verified by comparison with Bernoulli's equation and fluid dynamics equations relating pressure to volumetric flow through the orifice. The theoretical maximum velocity of the flow for a given driving pressure in the nozzle is calculated using Bernoulli's equation. Utilization of this equation assumed that there were no frictional or turbulent energy losses in the orifice and nozzle. The resulting equation was obtained by

$$P \approx \frac{\rho \cdot v_j^2}{2}$$

where P is the pressure in the nozzle measured by the transducer, v_j is the theoretical maximum jet velocity, and ρ is the liquid density. This method could also be used to determine the maximum instantaneous velocity of the jet.

Cryo-electron microscopy assay

For cryo-EM, frozen-hydrated specimens were prepared with a Thermo Fisher Vitrobot Mark IV plunger. The sample was placed on a glow discharge holey carbon grid (Quantifoil Au R1.2/1.3). The excess of solution from the grid was blotted for 3.0 s at 100% humidity at 8 °C before the grid was flash frozen in liquid ethane slush cooled at liquid-nitrogen temperature. Cryo-EM data were collected on a Thermo Fisher Titan Krios G3i electron microscope equipped with a Gatan K3 direct electron counting camera. The microscope was operated at 300 kV, and images of the specimen were recorded with a defocus range of − 1.4 to − 2.4 µm at a calibrated magnification of 64 k in the super-resolution mode of the K3 camera, thus yielding a pixel size of 0.54 Å on the object scale. A total of 2311 movie stacks, each containing 32 sub-frames, were recorded with the semi-automated low-dose acquisition program EPU, with a total accumulated dose of 50 electrons/Å2. The raw super-resolution dose-fractionated image stacks were 2 × Fourier binned, aligned, dose-weighted and summed using MotionCor2, resulting in summed micrographs in a pixel size of 1.08 Å. Contrast transfer function (CTF) parameters were estimated using CTFFIND4.1. Reconstruction resolutions were determined based on the gold-standard Fourier shell correlation (FSC) 0.143 criterion with the high-resolution noise.

Plasmid construction and preparation of mRNA

The full length spike with the KEN445 mutants (K417N-E484K-N501Y, KEN445) or the spike with the Omicron BA.5 mutants were synthesized respectively (Genscript, China). Both plasmids contained HBB 5'UTR, a CDS region encoding amino acid residues 1 through 1205 of the SARS-CoV-2 spike protein with the following mutations: a "GSAS" substitutions at the Furin cleavage site (residues 682–685), 6 proline substitutions at residues 817, 892, 899, 942, 986 and 987, and a C-terminal T4 fibritin trimerization motif, two tandem HBA2 3'UTR, 120 polyA tail. The sequences were cloned into a pUC57-kan vector. The mRNA encoding KEN445 mutants or BA.5 specific spike antigens were manufactured via in vitro transcription (IVT) with T7 RNA polymerase (Vazyme, China). Unmodified 5-triphosphate was completely replaced with N-1-methylpseudouridine-5-triphosphate (Synthgene, China). After IVT, the Cap-1 structure was added to the 5' terminus using vaccinia capping system and 2'-O- methyltransferase (Vazyme). The mRNA was purified with LiCl precipitation, resuspended in 1 mM sterile-filtered sodium acetate (pH 6.5), and kept frozen at − 80 °C until use.

LNP preparation, mRNA encapsulation and lyophilization

LNPs were prepared using the microfluidic technique. Ionizable cationic lipid (tricisionbio Biological Technology Co., Ltd. China), 1,2-distearoyl-sn-glycero-3-phosphocholine DSPC (AVT, China), cholesterol (AVT), polyethylene glycol lipid PEG (AVT, China) in ethanol were briefly combined with mRNA in pH 5.8 citrate buffer using a microfluidic mixer INano P (MicroNano, China). Formulations were then diluted and exchanged with 10 mM Tris (pH 7.0) containing series concentrations of sucrose. Formulations were concentrated using Amicon ultra-centrifugal filters EMD (Millipore, USA), and passed through a 0.22-μm filter, then transferred into vials. The vials were transported to the shelves of the freeze-dryer for lyophilization treatment. The size and zeta potential of mRNA-LNPs were monitored by dynamic light scattering (DLS) measurements using a Zetasizer Nano ZS (Malvern, USA). The encapsulation and concentration of mRNA were determined using the RiboGreen assay kit (Thermo Fisher).

Physicochemical analysis of mRNA-LNP particles upon NFI delivery

The lyophilized mRNA-LNP powder was reconstituted in nuclease-free water. The reconstituted samples were subsequently drawn into the NFI device. Then, the samples were injected (towards the bottom or at a 45º angle to the sidewall) into an eppendorf tube using the needle-free device with spring forces of 240 N, 320 N, 420 N, and 490 N. The untreated sample and the sample injected by traditional needle syringe were used as the blank and NI control samples, respectively. Finally, the size, PDI, and zeta potential of mRNA-LNP were analyzed with DLS. The encapsulation efficiency was measured using the RiboGreen assay.

Vaccination procedure

To assess the immunogenicity of the KEN445-mutant-mRNA-LNP vaccine (KEN445-LNP), BALB/c mice (4–6 weeks) were randomly allocated to groups and two intramuscular (IM) vaccinated using NI with a series of mRNA-LNP doses (0.02, 0.08, 0.3, 1.25, 5, 20 μg per mouse, n = 4), separated by a 4-week interval.

To compare effectiveness of different delivery methods, rats (5–7 weeks) were vaccinated intramuscularly with mRNA-LNP (5 or 10 μg per rat, n = 8) using either NFI or NI. For the multiple injection experiment, rats were vaccinated intramuscularly with 5 μg of mRNA-LNP at each injection site using NFI (one vaccination, two injections).

To compare effectiveness of different delivery methods, rabbits (4–6 months) were vaccinated intramuscularly or subcutaneously with 20 μg of mRNA-LNP per rabbit (n = 6), or 2 μg of BIBP inactivated vaccine (Sinopharm, China), or 10 μg of recombinant protein vaccine (SinoCellTech, China). Vaccinations were performed on day 0 and day 28. Unvaccinated control animals were administered an equivalent volume of 1 × PBS buffer. The sera were collected 7 and 14 days after each vaccination for all groups.

To assess the effectiveness of using BA5-LNP as a booster against Omicron BA.5 variants in heterogeneous vaccination, rabbits that have been primed with two doses of KEN445-LNP mRNA vaccine (tricisionbio, China), BIBP inactivated vaccine (Sinopharm, China), and recombinant protein vaccine (SinoCellTech, China) were vaccinated intramuscularly with a third dose of BA.5-LNP vaccine (tricisionbio, China) 2 months after the second immunization (20 μg per rabbit, n = 4).

Analyses of antigen-specific binding antibody

The antigen-specific binding antibody in serum was measured via ELISA. 5 μg/mL of full-length spike protein was coated into an ELISA plate overnight at 4 °C. After blocking with 2% BSA-TBST buffer, 100 μl of gradient-diluted serum were transferred to the 96-well plates and incubated for 2 h. Anti-Rat IgG F(ab)2-HRP secondary antibody (Sino Biological, China) or anti-Rabbit IgG Fc-HRP secondary antibody (Jackson ImmunoResearch, USA), both at a final concentration of 80 ng/mL, were added and incubated at 37 °C for 30 min. Plates were washed 5 times for subsequent color development reaction, which was carried out by adding tetramethylbenzidine substrates and terminated by 2 M H_2SO_4. Optical absorbance at 450 nm (OD_{450} nm) was recorded on a microplate reader (BioTek, USA). The concentration of binding antibody was calculated by a standard curve drawn based on the OD_{450} nm value of standard substance.

Angiotensin converting enzyme 2 (ACE2) inhibition assay

The antigen-specific neutralizing antibody in serum was measured with an ELISA-based ACE2 inhibition assay. Procedures were carried out according to the protocol provided by the Anti-SARS-CoV-2 Neutralizing Antibody Titer Serologic Assay Kit (ACRO Biosystems, China). 50 μl of gradient-diluted serum and 50 μl of SARS-CoV-2 spike RBD/protein were simultaneously transferred to the 96-well plate that was pre-coated with human ACE2 protein, incubating at 37 ℃ in a 5% CO_2 incubator for 1 h. After being washed three times, the microplate was patted dry. Then 100 μl of substrate and 50 μl of termination solution were added sequentially for the color development reaction. OD_{450} nm was subsequently recorded using a microplate reader (BioTek, USA). Antibody level was calculated using the following equation: ACE2 inhibition (%) = (1- sample OD_{450} nm/Negative Control OD_{450} nm) × 100%.

SARS-CoV-2 pseudovirus neutralization assay

The SARS-CoV-2 pseudovirus was manufactured by Sino Biological (Beijing, China). Huh-7 cell was obtained from the Chinese Culture Tissue Collection Center (CCTCC, China). The Luciferase Assay System and Passive Lysis 5 × Buffer were purchased from Promega (Madison, USA). For the quantitative measurement of neutralization antibodies, the SARS-CoV-2 pseudovirus PsV-Luc-Spike carrying the firefly luciferase gene was tested. Briefly, vaccine-immunized serum samples (deactivated at 56 °C for 30 min) were serially diluted, incubated with 200 $TCID_{50}$/well pseudovirus (1 h at 37 °C, in a 5% CO_2 incubator), and co-cultured with 2×10^4 cells for 20 h. Relative light unit (RLU) was measured to evaluate luciferase activity (CentroXS^3 LB 960 Microplate Luminometer). Inhibition rate of the pseudovirus entry was calculated as: Inhibition (%) = (Positive RLU - Sample RLU) / (Positive RLU - Negative RLU) × 100%. The pseudovirus neutralization titer (50% inhibitory dilution, $psVNT_{50}$) is defined as the serum dilution at which the RLUs were reduced by 50% when compared with the positive control wells. Positive neutralizing antibody (NAb) was determined to have greater than 50% inhibition, and the dose required to achieve this effect in 50% of the animals (ED_{50}) was calculated.

SARS-CoV-2 live-virus neutralization assay

The titers of neutralizing antibodies against SARS-CoV-2 were determined via the microplate cytopathic effect method in P3 lab (CDC, China). Serum samples were diluted in 96-well microtiter plates (Thermo) to appropriate concentrations, and then 100 $CCID_{50}$ (50% cell culture infectious doses) of SARS-CoV-2 were transferred to each pore, neutralizing at 37 ℃ in a 5% CO_2 incubator for 2 h. Next, applicable concentrations of Vero cells (Procell) were introduced and cultured at 37 ℃ in a 5% CO_2 incubator for 4 d, which further experienced cytopathic observation. Karber arithmetic was subsequently adopted for calculating the terminus of neutralization, namely the highest dilution of serum that could protect 50% of cells

against 100 $CCID_{50}$ challenge was the 50% plaque reduction neutralization titre ($PRNT_{50}$). The formula was summarized as $LogCCID_{50} = Xm + 1/2d - d \sum pi/100$, among which Xm = logarithm of the dilution of highest concentration of virus, d = logarithm of dilute coefficient, and $\sum pi$ = sum of the percentage of cytopathy per dilution. Live viruses of SARS-CoV-2 variants used in this study were Omicron BA.1 isolated from HongKong, Omicron BA.2 isolated from NingXia province, and Omicron BA.5 isolated from TianJin City of China, respectively.

Stability test

The lyophilized mRNA-LNP powder samples were stored at 4 ℃ and − 80 ℃ for 1 month, 2 months, 3 months and 6 months. The size, PDI, and zeta potential of the mRNA-LNP samples were analyzed with DLS. The encapsulation efficiency was measured using the RiboGreen assay.

Spike expression in vitro

2×10^4 A549 cells (CCTCC, China) were seeded in 96-well plates overnight. Then 0.3 μg of mRNA-LNPs with different storage time and storage temperatures were added into the plate. Post transfection 48 h, cell supernatants were harvested for Spike expression with ELISA kits (Sino Biological, China).

Statistical analysis

Statistical analysis was conducted using GraphPad Prism 8.3.0 Software. Two-way analysis of variance (ANOVA) and two-tailed unpaired *t*-test were used to test for statistical significance. Subject number and *p* values are marked in the figures. Quantitative image analysis of tissue distribution was conducted using ImageJ software.

Results

Study of fluid delivery via NFI in mammalian models

Since NI syringes rely on a closed tubular tunnel and human finger force to deliver liquid medicines, the resultant slow velocity renders formation of liquid aggregation at the injection site [28]. In contrast, the NFI system relies on instantaneously imposed spring-force and therefore is capable of creating high-velocity liquid jets at the outlet of the device, allowing diffusion of liquid medicines into the body through skin micro-pores [16]. Fig. 1 shows the models of intramuscular and subcutaneous delivery of mRNA-LNP particles via NFI. When an ultra-speed liquid jet stream passes through a skin micro-pore, a hierarchical resistance gradually slows down and disperses the liquid jet until it reaches the subcutis or muscle layer. The mRNA-LNP particles with dispersoid distribution in the delivery path are adequately exposed to immune cells that either existed locally or were recruited via blood or lymphatic circulation, including invading dermal DCs, Langerhans cells (LCs), and innate and effector immune cells [29]. With this in mind, we put forward a hypothesis that a finely-tuned NFI vaccine-delivery system could significantly boost immunogenicity compared to traditional NI-delivered vaccines.

As an initial proof of concept, we conducted an exploration in mammalian models. mRNA-LNPs containing methylene blue as an indicator were injected into the legs of rats and rabbits through NFI with gradient spring forces. After dissection, it was revealed that 200 N of spring-force was sufficient to deliver the liquid contents into the subcutaneous layer in rats, while 240 N allowed for intramuscular administration. NFI with 320 N spring force on rabbits achieved the same effect (Fig. 1c). Via NFI delivery, the diffusion areas of methylene blue in pork samples were measured to be 179 mm^2, 147 mm^2, 156 mm^2 and 131 mm^2 cross-sections upon the forces of 240 N, 360 N, 420 N and 490 N, respectively, that were significantly higher than NI groups (Fig. 1d). NFI provided better drug dispersion and distribution than NI in both the intramuscular and subcutaneous administrations. These findings confirm the feasibility of using NFI technology in mammals and have laid the foundation for the in vivo preclinical study of NFI-COVID-19 vaccine delivery systems.

Design and characterization of the mRNA-LNP vaccines

Among the SARS-CoV-2 spike mutation sites, K417N, E484A and N501Y (hereafter KEN445) in RBD are proven to be critical for vaccine escape, which are also shared by B.1.351 (β) and Omicron sublineages BA.1, BA.2, BA.5, BQ.1.1 and XBB [30–33]. In the present study, we adopted perfused conformation of the extracellular domain (ECD) of S protein as a skeleton, combined with additional furin and 6 P mutations and insertion of T4-fibritin (FT) trimerization motif at C-terminus to construct KEN445 mutants or BA.5-mRNA sequence (Fig. 2a). This strategy enabled and guaranteed the successful translation of S protein and its stabilization [34–36]. Next, the LNP comprised of ionizable lipid-C2, DSPC, Cholesterol and PEG-lipid [37,38] was synthesized for encapsulating mRNA. The resultant mRNA-LNP was further surrounded by sucrose to form intact systems, namely the two mRNA vaccines, KEN445-LNP and BA.5-LNP covered in the present study (Fig. 2b).

Using ELISA, we discovered that the serum from KEN445-LNP vaccinated mice could bind the receptor-binding domain (RBD) or inhibit binding to ACE2. Indeed, KEN445-LNP vaccinated mice induced potent RBD-specific antibodies (Fig. 2c) and blocked ACE2 binding (Fig. 2d). Binding to the full length spike was assessed in Fig. 2d, because a potential benefit of targeting the full length spike instead of RBD is the induction of a polyclonal antibody response that recognizes multiple epitopes, thus avoiding immune escape by antigenic drift. Neutralizing activity was measured using a pseudovirus neutralization assay and a live virus plaque reduction neutralization assay. Reciprocal 50% pseudovirus neutralization geometric mean titers ($psVNT_{50}$ GMTs) increased significantly with a dose-dependent trend, from 286 to 23,660 (Fig. 2e). Mice vaccinated with 20 μg of KEN445-LNP had GMTs of 308 for Omicron BA.1 and 800 for Omicron BA.2 respectively in live virus neutralization test (Fig. 2f).

Taken together, KEN445-LNP, delivered via NI, induced robust S-specific antibody responses with potent neutralizing capacity against SARS-CoV-2 Omicron variants.

Stability of mRNA-LNP particles subjected to NFI

LNP nanospheres have been widely used in mRNA vaccines and medicines to protect and transport mRNA species into cells. Stability of LNP nanospheres has been a limiting factor on commercialization of mRNA-type vaccines [39]. Therefore, it is of great interest to study whether LNP nanospheres can survive the severe NFI operation conditions. Herein, after optimization of NFI parameters, we used an NFI device to deliver normal saline-dissolved mRNA-LNP, which has been determined to possess long-term stability for 6 months at 2–8 °C (Fig. 3d), and described three possible outcomes for the mRNA-LNP particles: distribution, aggregation, or destruction (Fig. 3a). Firstly, we monitored the flow velocity of mRNA-LNP at the positions of 8 mm, 2 mm, and 0.02 mm relative to the outlet of the NFI device. Unexpectedly, a high speed of 140 m/s was observed near the outlet even at 240 N spring force, whereas the force of 490 N increased the speed to 202 m/s (Fig. 3b). To elucidate whether the structure of the KEN445-LNP particle would be disrupted after NFI, we conducted physicochemical analyses. Under the established injection conditions for humans, the diameter of the NFI-based

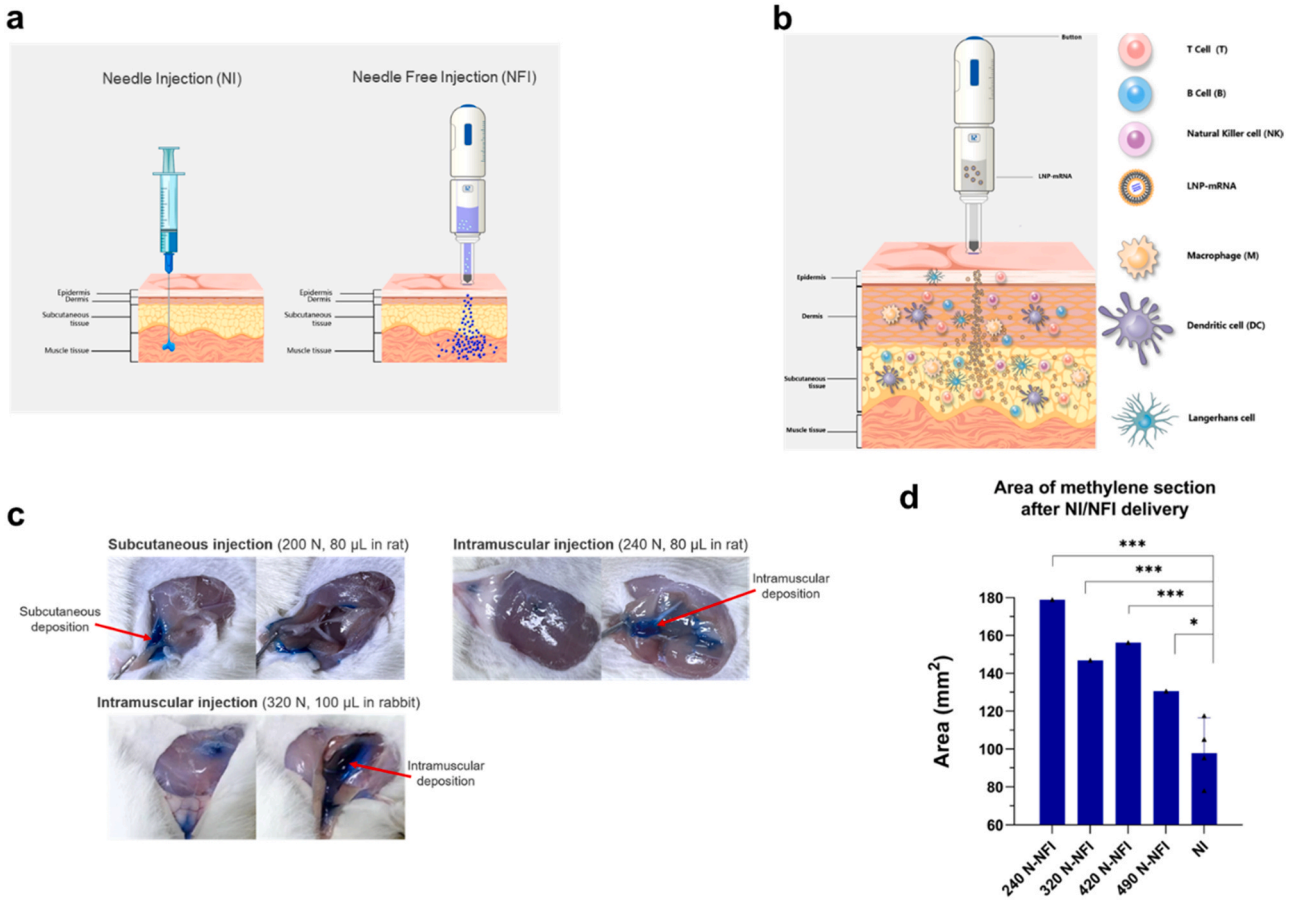

Fig. 1. Schematic diagram and applied exploration of NFI-mRNA-LNP in mammalian models. (a) Comparison of NFI and NI in intramuscular administration. The dispersoid distribution of mRNA-LNP injected by NFI facilitates better absorption and entry into cells compared to that injected by NI. (b) A model illustrates the process of subcutaneous injection of mRNA-LNP with NFI. With the canonical NI system, delivery microparticles were believed to frequently form aggregations. In contrast, NFI is capable of dispersing mRNA-LNP particles in the delivery path, which allows for increased exposure to various kinds of immune cells. (c) Representative pictures for NFI deliveries in rats and rabbits. mRNA-LNP containing methylene blue was delivered to explore the optimum spring force for intramuscular or subcutaneous delivery (n = 4). Pictures were taken focusing on the injection site of legs. (d) Quantification analysis of mRNA-LNP dispersion areas after NI/NFI deliveries. mRNA-LNPs containing methylene blue were delivered to the muscle layer of the skin. The areas containing methylene blue were quantitatively analyzed by ImageJ Software. * : $P < 0.05$; * *: $P < 0.01$; * ** : $P < 0.001$. Statistical analyses were performed using GraphPad Prism 8.3.0 software.

KEN445-LNP was observed to have no differences in comparison to the re-dissolved one. When the vaccine was injected directly with maximum pressure, the mean values of the particle size of each panel invariably stayed at a range of 160–220 nm (Fig. 3c). On the same experimental subjects, polydispersity index, zeta potential and encapsulation efficiencies kept at ranges of below 0.3, 30–45 mV, and over 80%, respectively, indicating that the KEN445-LNP particles maintained stability in the face of strong Eppendorf tube interactions created by the high flow velocity. In addition, using a 45° injection angle relative to the tube wall, simulating in vivo physiological conditions of mRNA-LNP into the tissue, achieved the same stability (Fig. 3c).

To further study the status of KEN445-LNP particles after NFI delivery, we used cryo-electron microscopy (cryo-EM) to visualize the appearance of particles. Compared to NI-delivered particles, 320 N NFI-delivered particles retained similar aspects, clear LNP structures, and equal embedded mRNAs. These results were consistent with the aforementioned physicochemical analyses. Although the imposition of high pressure via NFI slightly promoted the separation of LNP and mRNA molecules, intact KEN445-LNP particles still dominated the population (Fig. 3d and c), indicating the constitution of KEN445-LNP was practically resistant to the forces introduced by NFI devices.

Humoral immune responses induced by NFI- and NI-delivered KEN445-LNP in rats

Given the decent immunogenicity of KEN445-LNP in mice, we further asked whether NFI-based administration of this vaccine could elicit equivalent or better protective efficacy against SARS-CoV-2 compared to the NI approach. Omicron mutants were picked to test the cross-protection generated by KEN445-LNP. As expected, NFI- and NI-delivered 5 μg vaccines, after two times of vaccination, induced similar levels of spike-specific binding antibody, with no statistically significant differences. The results with 10 μg vaccine doses suggested similar outcomes. It is noteworthy that both dosages reached a LOD (limit of detection) at concentrations over 10^5 ng/mL, regardless of whether delivered via NI or NFI (Fig. 4a and b). Moreover, 1 week after the 2nd vaccination, both NFI- and NI-delivered 10 μg dosages acquired results with lower standard deviations than the 5 μg dosages, and the binding antibody 2 weeks after the 2nd vaccination presented a similar phenomenon.

Generation of $psVNT_{50}$ serum titers against Omicron-BA.1, 7 days and 14 days after the 2nd vaccination with KEN445-LNP, were measured using the pseudovirus neutralization assay. A similar result to the binding antibody assay was obtained in the test using the Omicron BA.1-pseudovirus (Fig. 4c and d), indicating that NFI- and NI-delivered KEN445-LNP harbored equivalent immunogenicity and cross-protection in rats. Again, 10 μg vaccine injections induced

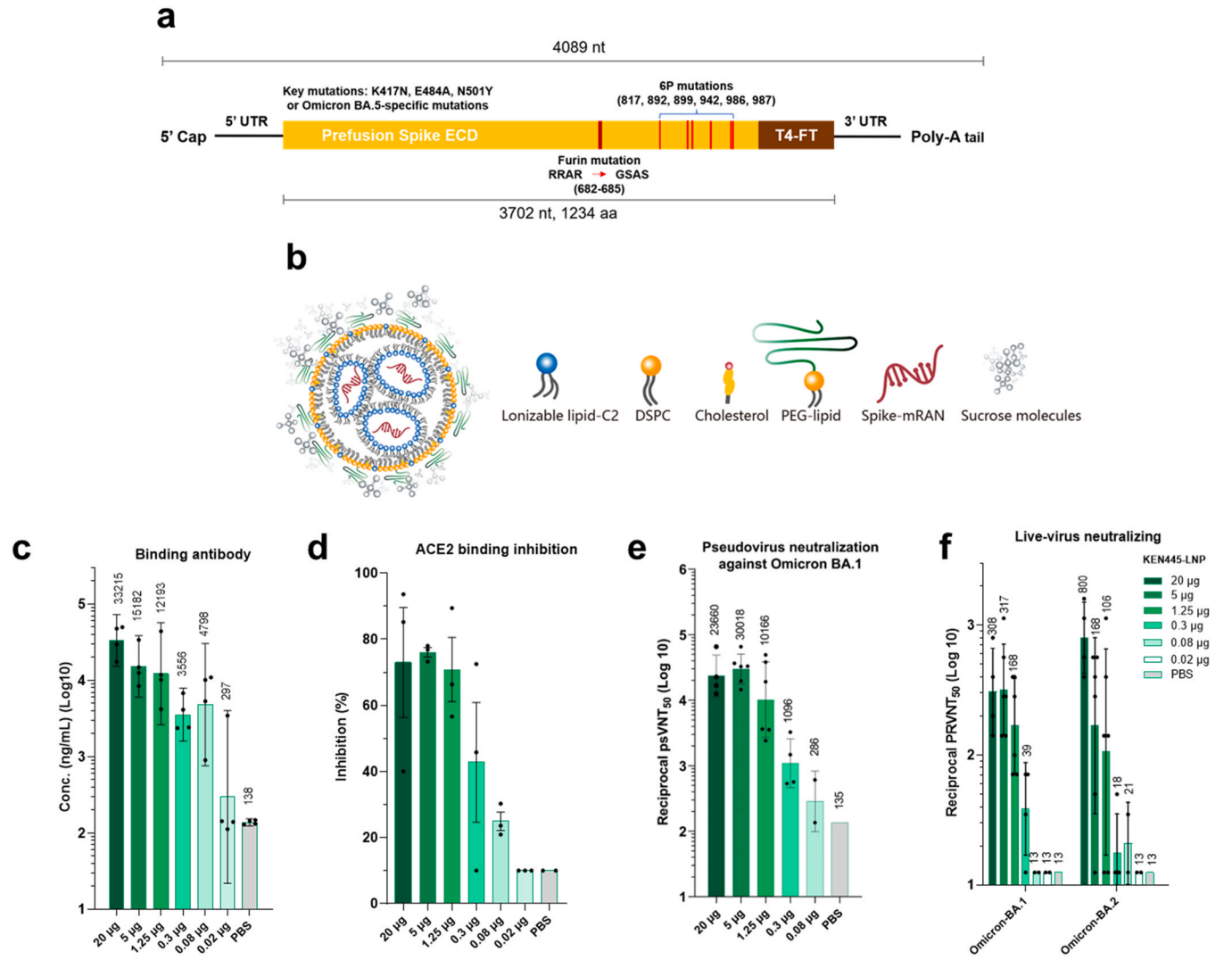

Fig. 2. Humoral immune response induced by NI-KEN445-mRNA-LNP in mice. (a) Schematic diagram of KEN445-mRNA and BA5-mRNA sequence. The coding region was designed according to the DNA sequence of SARS-CoV-2 spike protein, including the critical mutations of K417N, E484A and N501Y or Omicron BA5 specific mutations. The specific positions of mutations were described relative to the sequence of the wild type S protein. (b) Molecular diagram of mRNA-LNP system. Sucrose was employed as a protective agent against oxidation of LNP particles. (c - f) SARS-CoV-2 Spike specific binding antibodies (c) and neutralizing activity (d), cross protection against the Omicron-BA.1 variant (e), and neutralization of Omicron-BA.1 and BA.2 live viruses (f) induced by KEN445-LNP doses were determined using ELISA and ACE2 inhibition assays, a pseudovirus-based neutralization assay (50% pseudovirus neutralization titer , $psVNT_{50}$) and a live-virus neutralization assay (50% plaque reduction neutralization titer, $PRNT_{50}$). Serum samples were collected 14 days after the second vaccination. Statistical analyses were performed using GraphPad Prism 8.3.0 software (n = 4). The mean value of each individual on the X axis is shown above the column in figure c. A reciprocal 50% neutralization titer (NT_{50}) geometric mean titer (GMT) is shown above the column in Fig. e and f.

higher levels of $psVNT_{50}$ and lower standard deviations than the 5 μg vaccine injections. In addition, production of RBD-specific binding antibodies at 7 days and 14 days after the 2nd vaccination with KEN445-LNP through NFI administration using a series of a 5 μg dose at a single position, a 10 μg dose at a single position, and two 5 μg doses simultaneously at two different skin positions (total 10 μg) were also examined. At 1 week or 2 weeks after the 2nd vaccination, all three dosing methods reached maximum level of antibody (LOD). Again, measured with standard deviation, the single 10 μg dose injection significantly reduced the variation of the immune response results compared to the single 5 μg dose. When a 10 μg dose was divided into two 5 μg doses and injected into two separate positions simultaneously, a further reduction of standard deviation was observed (Fig. 4e and f). Dividing a single dose into multiple smaller doses followed by the simultaneous delivery to different positions is a unique design that the NFI system could easily achieve, and could be a more favorable vaccination method for people with low immune responses. Further study on this topic is ongoing.

Omicron BA.5-specific neutralizing antibody induced by NFI-delivered mRNA-LNP vaccines in rabbits

Considering that Omicron sublineages has become the prominent variant at present [40], we subsequently probed whether an additional dose of NFI-delivered BA.5-LNP following two doses of NI- or NFI-delivered KEN445-LNP was capable of providing cross-protection against the Omicron BA.5 variant in rabbits. Neutralizing activities were measured through a live-virus neutralization assay. Serum samples were collected 7 days after the 2nd vaccination and 14 days after the 3rd vaccination in rabbits. NFI-delivered KEN445-LNP induced generation of 5.3-times more BA.5-specific neutralizing antibody than the NI-delivered KEN445-LNP, and this enhancement of immunogenicity was statistically significant (Fig. 5a). Similarly, NFI-mediated booster vaccinations of either inactivated or recombinant protein vaccines strongly increased the BA.5-neutralizing antibodies compared to NI operation (Fig. 6b). Using the highly efficient BA.5-LNP as the third dose on mismatched samples (to even the starting level of neutralizing antibody) quickly induced the

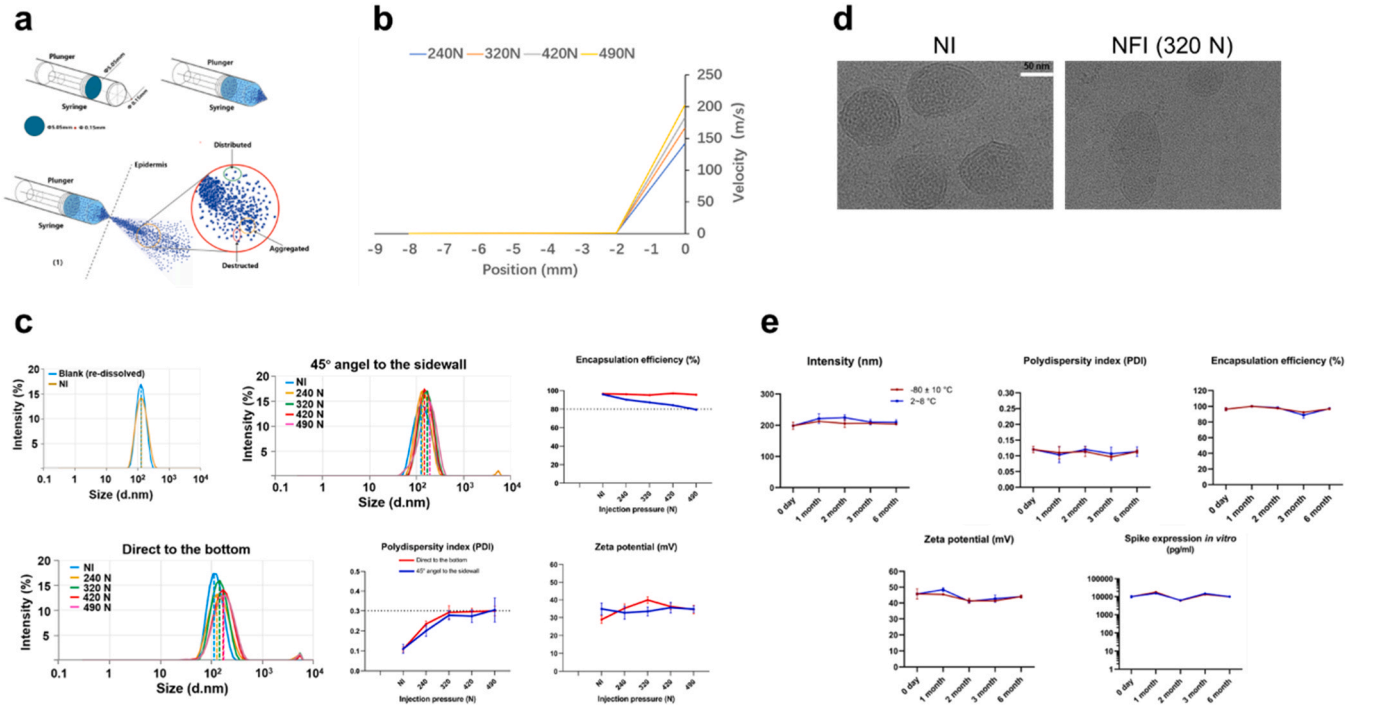

Fig. 3. Dynamics of physicochemical characteristics of KEN445-LNP upon NFI delivery. (a) Abridged general views of the NFI process. mRNA-LNP particles are distributed, aggregated, or destroyed through NFI delivery. (b) Flow velocity of KEN445-LNP generated by a gradient of increasing pressure in the NFI system. The origin represents the outlet of the NFI device. Position represents the testing point of flow velocity. (c) Physicochemical parameters of mRNA-LNP particles after NFI delivery within 240 N, 320 N, 420 N, 490 N. Polydispersity, diameter, zeta potential, and encapsulation efficiency of mRNA-LNP upon augmentation of pressure, with and without a 45° angle to the sidewall. Statistical analyses were performed using GraphPad Prism 8.3.0 software (n = 5). (d) Cryo-electron micrographs of mRNA-LNP particles treated by NFI and NI. The representative pictures were selected at a view size of 81 K. Scale bar: 50 nm. (e) Long-term stability of KEN445-LNP. Intensity, PDI, encapsulation efficiency, zeta potential and spike expression in vitro of KEN445-LNP particles were measured after storage at −80 ± 10 °C or 2–8 °C for 0 days to 6 months. Statistical analyses were performed using GraphPad Prism 8.3.0 software (n = 3).

maximum amount of BA.5-specific neutralizing antibodies, regardless of if given via NI- or NFI-delivery. Both NI- and NFI- panels achieved a plateau for induing antibodies against Omicron BA.5 and showed no significant difference statistically (Fig. 5a). The neutralizing antibodies were also confirmed via an ACE2 inhibition assay using 50 times diluted-serum samples since ACE2 is the major receptor of SARS-CoV-2 S protein [41–43]. A third dose of BA.5-LNP via NFI-delivery induced 3.70 times higher level inhibition of Omicron BA.5-ACE2 binding (Fig. 5b). Again, this immune enhancement was statistically significant. Altogether, the NFI delivery system in rabbits displayed superior vaccination responses than the NI delivery system. In addition, BA.5-LNP exhibited a strong boosting capability in reinforcing the immune responses of mammals against the Omicron BA.5 variant.

Beyond that, we further queried whether the routes of administration would be responsible for some distinct consequences. $psVNT_{50}$ titers against Omicron-BA.5, 14 days after both the 3rd NFI-vaccination of BA.5-LNP (Fig. 5c) and the 3rd NI-vaccination of KEN445-LNP (Fig. 5d) through both subcutaneous and intramuscular injections, were determined in rats, which revealed that subcutaneous injections induced a higher level of vaccination response than intramuscular injections. It was also interesting to note that NFI-delivery produced results with higher variability.

Interactions between BA.5-LNP and other types of vaccines for induing Omicron BA.5-specific neutralizing antibodies

To further confirm the capability of BA.5-LNP in protecting against the Omicron BA.5 variant, we next conducted an ACE2 inhibition assay (Fig. 5b) in rabbits that had previously received two vaccinations with inactivated or recombinant protein vaccines. After the third vaccination of BA.5-LNP, $PRNT_{50}$ GMT all reached upper LOD (Fig. 5a), which demonstrated the superior immunity-boosting capability of BA.5-LNP. In order to detect the differences of immune responses among subjects previously administered various types of vaccines, the serum samples were diluted 50 times to reach the lower-level detection limit. After a conversion, heterogeneously NFI-mediated BA.5-LNP was observed to increase the Omicron BA.5-specific neutralizing activity in inactivated vaccine-based rabbits by about 3.95 times, in recombinant protein vaccine-based rabbits by 2.75 times (Fig. 6), and in mRNA vaccine-based rabbits by 3.70 times (Fig. 5b). These results have together shown an apparent immunity-boosting effect thus emphasizing the application of BA.5-LNP in the real world for promoting the cross-protection against Omicron BA.5 in those who have received various combinations of COVID-19 vaccines. Cross protection results and discussions will be detailed in a separate paper for future submission.

Discussion

Nearly three years of havoc caused by the COVID-19 pandemic has brought about incalculable damage to human society [44–46]. To some extent, the emergence of various vaccines has curbed the spread of SARS-CoV-2 and established a primary immune barrier [47,48], but this fragile balance is being constantly disrupted by the rapid evolution of various novel variants [49,50]. The development of effective vaccines has always lagged behind the rate of virus mutation. Therefore, two strategies, heterologous and booster vaccinations, have been proposed to maintain an effective level of antibodies and provide cross-protection against VOCs on the basis of available vaccines [51–54]. In both strategies, COVID-19 vaccination must become a routine practice. In this study, we took inspiration from the commercial usage of NFI devices among diabetics [55] to introduce the NFI system to COVID-19 vaccines, with addressing

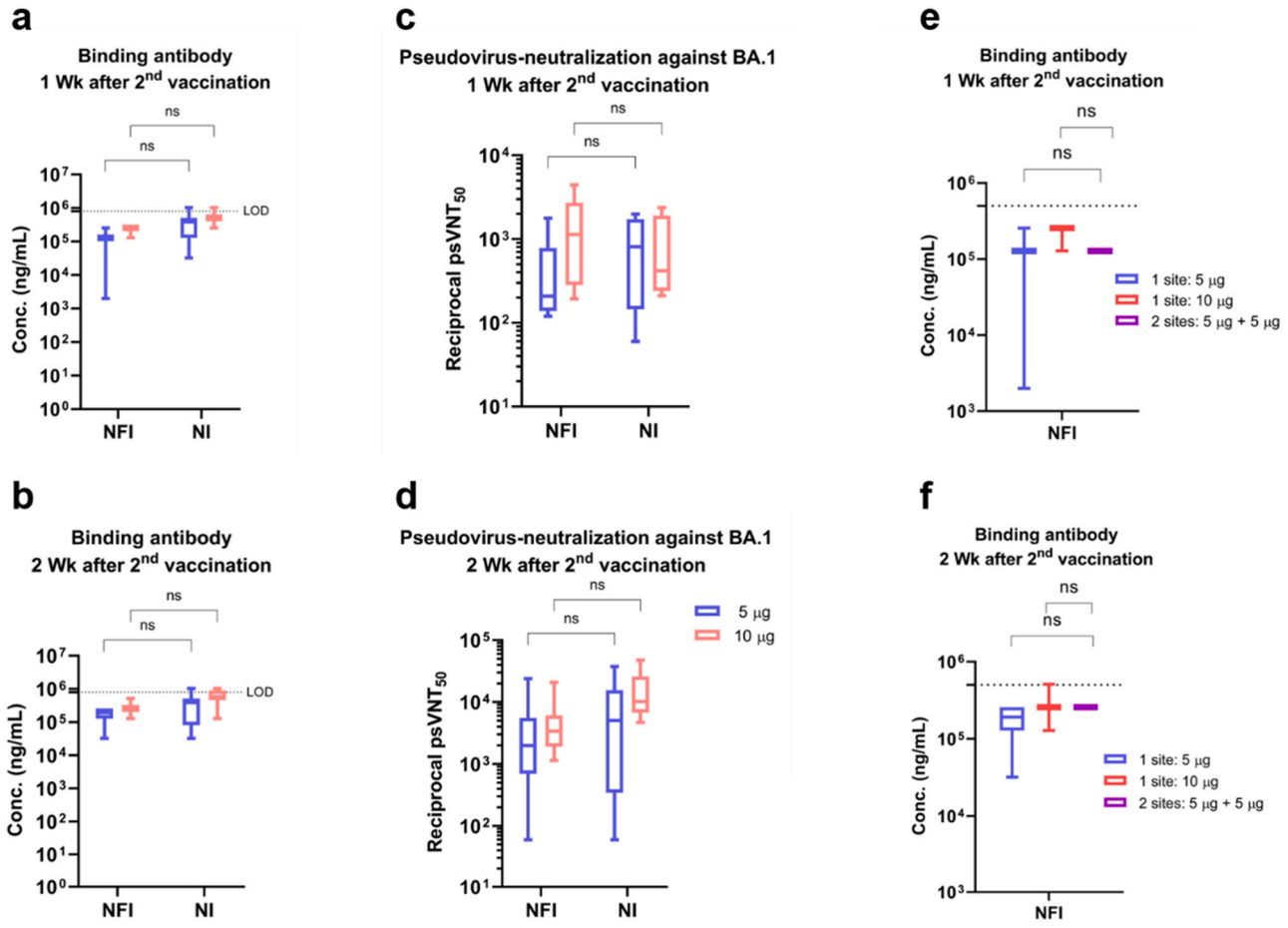

Fig. 4. Humoral immune response induced by KEN445-LNP vaccines after NFI and NI administrations in rats. (a, b) Binding antibodies against S RBD at 7 days (a) and at 14 days (b) after the 2nd vaccination were measured using ELISA method. (c, d) $psVNT_{50}$ serum titers against Omicron-BA.1 at 7 days (c) and 14 days (d) after the 2nd vaccination were determined by a pseudovirus neutralization assay. (e, f) RBD-specific binding antibody at 7 days (e) and 14 days (f) after the 2nd vaccination with a strategy of 2 injections totaling a 10 μg dose (5 μg + 5 μg) during one vaccination. (a - f) Statistical analyses were performed using GraphPad Prism 8.3.0 software (n = 8; ns means: not significant).

needle phobia as the original purpose. We selected a type of QS-P NFI-device manufactured by Quinovare as a tool, after optimization, to test the effectiveness of two designed LNP-based mRNA vaccines against SARS-CoV-2. We proposed that the dispersion of high-flow velocity particles within the tissue after NFI-delivery would enhance immunogenicity of mRNA-LNP via increased interaction with immune cells (Fig. 1a and b). We first deciphered the optimal pressure required for NFI-delivery through different routes in rat and rabbit models (Fig. 1c and d). Next, we described the strategy for constructing the SARS-CoV-2-specific mRNA vaccines covered in this study (Fig. 2a and b), of which KEN445-LNP was suggested to generate high immunogenicity and effective cross-protection (Fig. 2c-f).

An essential prerequisite for effective mRNA vaccines is to ensure abundant mRNA entering the cells efficiently [56]. The poor resistance of LNP to the physical stresses imposed by the freeze-drying process [57,58] has suggested that even a minimum flow velocity of NFI might be sufficient to cause collision of mRNA-LNP particles and destruction by breaking or aggregation. To our surprise, all the physicochemical parameters and cryo-EM images have revealed that an optimized NFI system keeps the conformation of KEN445-LNP stable, even at the highest force of 490 N for human NFI injections (Fig. 3c and d). In addition to our NFI system optimization, a possible reason for this favorable stability was that the sucrose, which was utilized as antioxidant, further protected the mRNA-LNP system from high-speed and high-pressure impact. The refined selection and ratio of raw materials within our LNPs could also be an explanation. Further research will be conducted to investigate this stability.

With the confirmation of stability of the designed mRNA-LNP particle upon NFI delivery, we next conducted a comparison of immunogenicity generated by NFI- and NI-delivery in mammalian models. In contrast to the equivalent immune responses yielded by NFI and NI in rats, NFI-delivered KEN445-LNP in rabbits, a species that is 10–15 times larger than rats, exhibited a higher immune response compared to NI-based delivery (Fig. 4a-d; Fig. 5a). A similar immunogenic result of the comparison between NFI and NI was also obtained when using inactivated and recombinant protein vaccines in rabbits (Fig. 6a). We conjecture that the size difference between the model animals is the origin of this different immune response. Specifically, the dispersing effect from NFI delivery, which promotes more contact of mRNA-LNP particles to immune cells, is likely limited in small mammals. In relatively larger mammals, the more ample spatial distribution of immune cells allows the dispersed mRNA-LNP particles to play a more prominent role in antibody production. Conduction of primate tests are necessary to verify this hypothesis and lead to further human clinical studies. Additionally, subcutaneous administration of mRNAs-LNP at the third vaccination created a higher level of cross-protection than intramuscular administration against Omicron BA.5-live virus in rats, for both NFI-based BA.5-LNP and NI-based KEN445-LNP deliveries (Fig. 4e and f). The results suggest that mRNA-LNP vaccines are better delivered by subcutaneous injection because of the increased interaction with immune cells [18,29]. On the topic of strengthening cross-protection

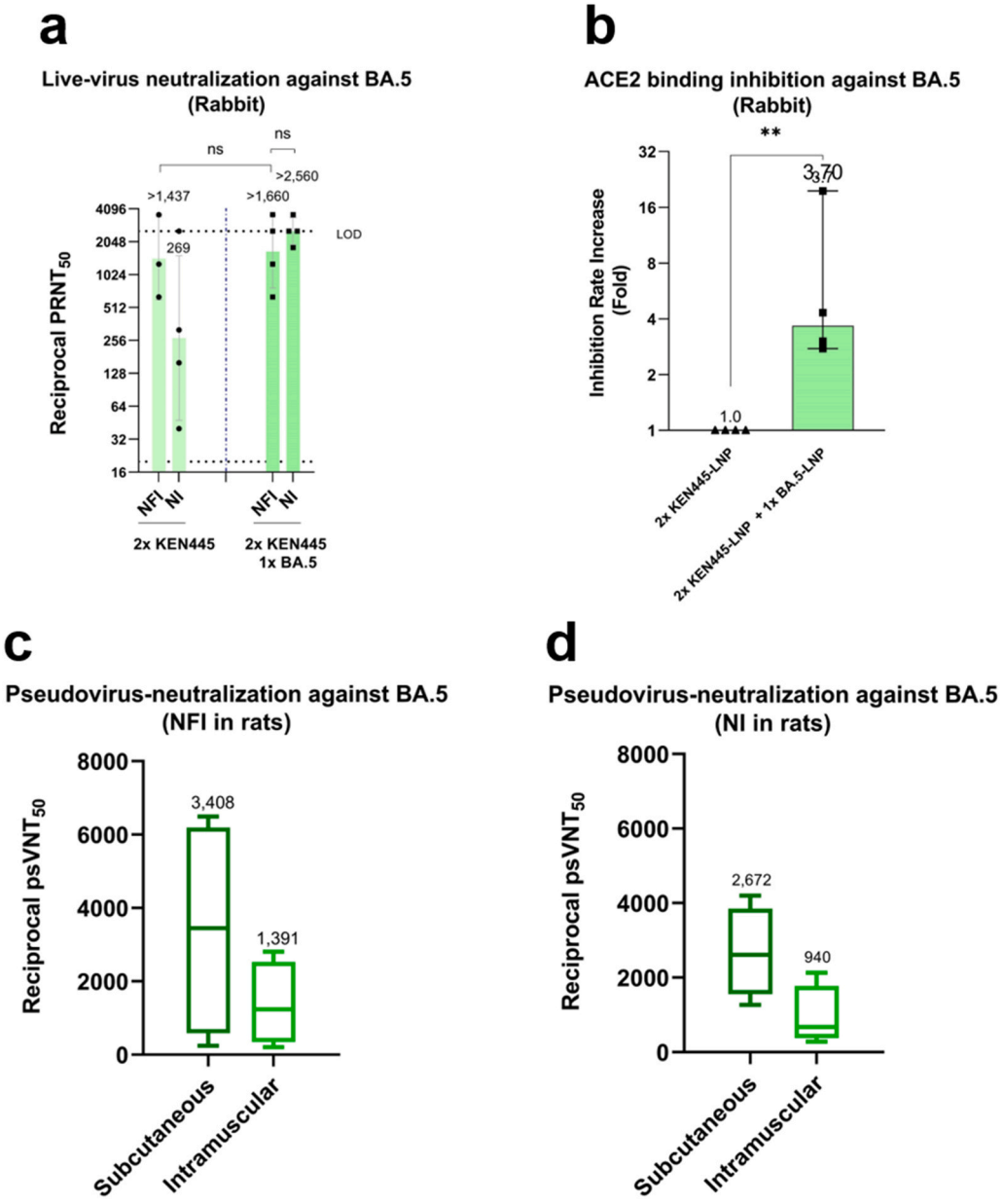

Fig. 5. Omicron BA.5-specific neutralizing antibodies induced by mRNA-LNP vaccines with NFI. (a) $PRNT_{50}$ serum titers against Omicron-BA.5 after two vaccinations with KEN445-LNP and heterogeneous enhancement by BA.5-LNP in rabbits. A live-virus neutralization assay was adopted. (b) Comparison of ACE2-Omicron BA.5 inhibition rate between twice-vaccinated and heterogeneously enhanced NFI panels. Serum samples were the same batch as (a) with further dilution process. Inhibition rate increase was calculated using the value of the 2nd vaccination as a standard (Fold changes). (a, b) Serum samples were collected at 7 days after the 2nd vaccination and at 14 days after the 3rd vaccination in rabbits. (c, d) $psVNT_{50}$ serum titers against Omicron-BA.5 at 14 days after the 3rd NFI-vaccination of 10 μg BA.5-LNP (c) and 3rd NI-vaccination of 10 μg KEN445-LNP (d) through subcutaneous and intramuscular injections were determined by pseudovirus neutralization assay in rats. The subjects were previously vaccinated twice with 10 μg KEN445-mRNA. (a - d) Statistical analyses were performed using GraphPad Prism 8.3.0 software (n = 4; **: $P < 0.01$). A reciprocal 50% neutralization titer (NT_{50}) geometric mean titer (GMT) is shown above the column in figure a, c and d.

against the Omicron BA.5 variants by heterogeneous vaccination of BA.5-LNP, we observed that the value of $PRNT_{50}$ GMT plateaued after two vaccinations of NFI-based KEN445-LNP in rabbits. Furthermore, the 50 times-diluted serum samples from the same batch displayed significant suppression of Omicron BA.5-ACE2 binding after using NFI-delivered BA.5-LNP at the third vaccination (Fig. 5a and b), indicating that the BA.5-mRNA, which was constructed by employing the S protein sequence of Omicron BA.5 as a skeleton, was indeed able to reinforce the cross-protection against Omicron BA.5 heterogeneously. Moreover, we have also made an effort to decrease individual variations in immune responses to mRNA-LNP drugs when using NFI delivery, and put forward a protocol of split injections of a single dose at different sites during one vaccination (Fig. 4g and h). The decreased variability was the result of increasing antibody levels in subjects with lower immune responses to the upper LOD. We suggest that this increased consistency is due to the greater mRNA-LNP dispersion.

Finally, since the highly effective mRNA COVID-19 vaccines were only partially used world-wide, heterogeneous vaccination across different types of vaccines using distinct delivery methods would be an ideal solution for combating the rapidly mutating SARS-CoV-2 virus. Our results suggest that NFI-delivered BA.5-LNP could be chosen as an effective booster for people who were previously vaccinated with inactivated, recombinant protein, or mRNA vaccines (Fig. 6), broadening our knowledge of the consequences of interactions between different COVID-19 vaccines.

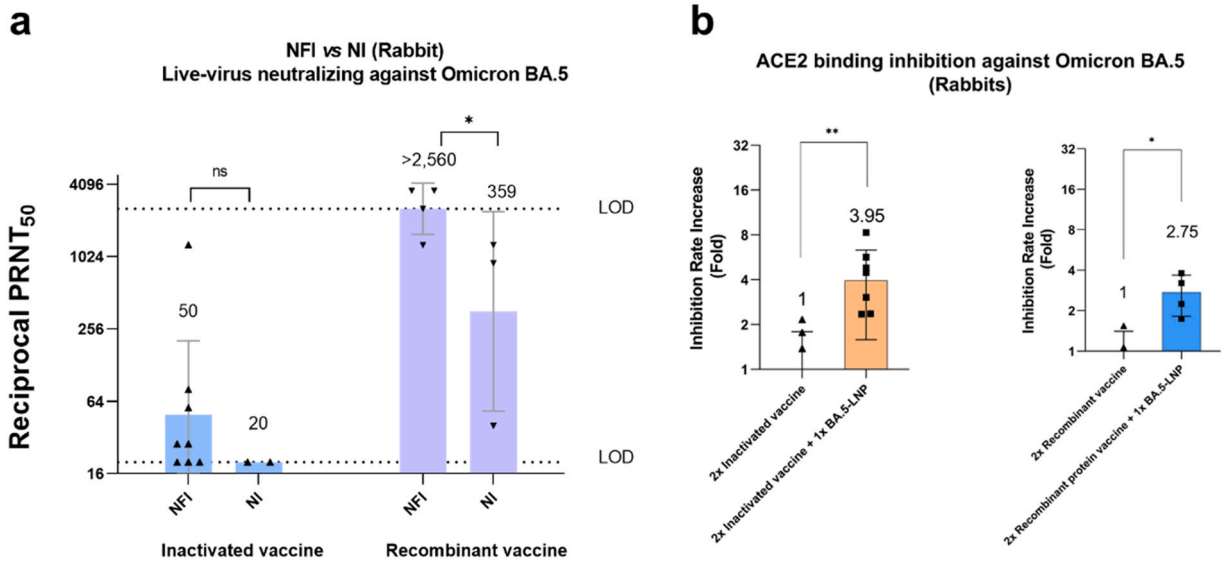

Fig. 6. Omicron BA.5-specific neutralizing antibodies induced by inactivated vaccine and recombinant protein vaccine with NFI. (a) Serum-neutralizing capacity of the rabbits immunized with inactivated and recombinant protein vaccines delivered by NFI and NI. $PRNT_{50}$ serum titers against Omicron-BA.5 after two vaccinations with 2 μg inactivated and 10 μg recombinant protein vaccines were measured through live-virus neutralization assay. Serum samples were collected 7 days after the 2nd vaccination. Inactivated vaccine group: NFI (n = 8), NI (n = 2); Recombinant protein vaccine group: NFI (n = 4), NI (n = 3); *: $P < 0.05$; ns means: not significant. A reciprocal 50% neutralization titer (NT_{50}) geometric mean titer (GMT) is shown above the column in figure a. (b) Enhancement of Omicron BA.5-specific neutralizing antibodies after the 3rd NFI-vaccination of BA.5-LNP. Neutralizing antibodies induced by NFI-delivery through intramuscular administration were confirmed via ACE2 inhibition assay. Serum samples were collected 7 days after the 2nd vaccination and 14 days after the 3rd vaccination in rabbits, which were processed with further dilutions to reach the neutralizing antibody lower detection limit. Inhibition rate increase was calculated using the value of the 2nd vaccination as a standard (Fold changes). Statistical analyses were performed using GraphPad Prism 8.3.0 software. Inactivated vaccine group: n = 8, **: $P < 0.01$; Recombinant protein vaccine group: n = 4, *: $P < 0.05$. The mean value of each individual on the X axis is shown above the column.

5. Conclusions

With this study, we have discovered and explained some important phenomena associated with the use of NFI devices as an mRNA-LNP vaccine delivery system. Firstly, NFI-based delivery systems could provide better immunogenicity than NI-based delivery systems. Secondly, BA5-LNP could be used as an effective booster for vaccination against the Omicron BA.5, following a variety of different types of vaccines such as inactivated, recombinant protein, and mRNA vaccines. Thirdly, split injections of a single dose at different sites during one vaccination could be a more effective protocol in future vaccination. Fourthly, an optimized NFI system allows for minimal destruction of mRNA nanoparticles, which opens the door for application of the NFI system in a wide variety of vaccine and drug deliveries.

Funding

This work was supported by Beijing Municipal Science & Technology Commission [z211100002521025].

CRediT authorship contribution statement

Shanhong Mao: Conceptualization, Writing – review & editing. **Shiyou Li:** Data curation, Writing – review & editing. **Yuxin Zhang:** Conceptualization; **Luoxin Long:** Methodology. **Junfeng Peng:** Writing – original draft, Data analysis. **Yuanyan Cao:** Methodology. **Jessica Z Mao:** Writing – review & editing; **Xin Qi:** Investigation. **Qi Xin:** Investigation. **Guoliang San:** Methodology. **Jing Ding:** Investigation. **Jun Jiang:** Investigation. **Xuejiao Bai:** Investigation, Methodology. **Qianting Wang:** Methodology. **Pengfei Xu:** Investigation. **Huan Xia:** Data analysis. **Lijun Lu:** Drawing. **Liangzhi Xie:** Reviewing. **Desheng Kong:** Investigation. **Shuangli Zhu:** Investigation. **Wenbo Xu:** Supervision, Investigation.

Data Availability

Data will be made available on request.

Declaration of Competing Interest

The authors declare the following financial interests/personal relationships which may be considered as potential competing interests: Shiyou Li, Jun Jiang, Qi Xin, Junfeng Peng, Huan Xia, Lijun Lu, Qianting Wang, Xuejiao Bai, Pengfei Xu reports financial support was provided by Beijing Municipal Science and Technology Commission.

Acknowledgement

Thanks to Dr. Fu Gao and Professor Xiaoliang Xie for the valuable discussions. Thanks to Professor Lindsey M. F. Mao, Department of Biological Sciences, Benedictine University of Illinois, USA for proveeading and valuable comments on this manuscript. Thanks to Ms. Peggy Chen for the valuable discussions.

References

[1] Q. Huang, J. Zeng, J. Yan, COVID-19 mRNA vaccines, J. Genet. Genom. 48 (2021) 107–114.
[2] D.A. Collier, A. De Marco, I.A.T.M. Ferreira, B. Meng, R.P. Datir, A.C. Walls, S.A. Kemp, J. Bassi, D. Pinto, C. Silacci-Fregni, S. Bianchi, M.A. Tortorici, J. Bowen, K. Culap, S. Jaconi, E. Cameroni, G. Snell, M.S. Pizzuto, A.F. Pellanda, C. Garzoni, A. Riva, CITIID-NIHR BioResource COVID-19 Collaboration, A. Elmer, N. Kingston, B. Graves, L.E. McCoy, K.G.C. Smith, J.R. Bradley, N. Temperton, L. Ceron-Gutierrez, G. Barcenas-Morales, COVID-19 Genomics UK (COG-UK) Consortium, W. Harvey, H.W. Virgin, A. Lanzavecchia, L. Piccoli, R. Doffinger, M. Wills, D. Veesler, D. Corti, R.K. Gupta, Sensitivity of SARS-CoV-2 B.1.1.7 to mRNA vaccine-elicited antibodies, Nature 593 (2021) 136–141.
[3] D. Zhou, W. Dejnirattisai, P. Supasa, C. Liu, A.J. Mentzer, H.M. Ginn, Y. Zhao, H.M.E. Duyvesteyn, A. Tuekprakhon, R. Nutalai, B. Wang, G.C. Paesen, C. Lopez-Camacho, J. Slon-Campos, B. Hallis, N. Coombes, K. Bewley, S. Charlton, T.S. Walter, D. Skelly, S.F. Lumley, C. Dold, R. Levin, T. Dong, A.J. Pollard, J.C. Knight, D. Crook, T. Lambe, E. Clutterbuck, S. Bibi, A. Flaxman, M. Bittaye, S. Belij-Rammerstorfer, S. Gilbert, W. James, M.W. Carroll, P. Klenerman, E. Barnes, S.J. Dunachie, E.E. Fry, J. Mongkolsapaya, J. Ren, D.I. Stuart,

G.R. Screaton, Evidence of escape of SARS-CoV-2 variant B. 1.351 from natural and vaccine-induced sera, Cell 184 (2021) 2348–2361.
[4] E.C. Wall, M. Wu, R. Harvey, G. Kelly, S. Warchal, C. Sawyer, R. Daniels, P. Hobson, E. Hatipoglu, Y. Ngai, S. Hussain, J. Nicod, R. Goldstone, K. Ambrose, S. Hindmarsh, R. Beale, A. Riddell, S. Gamblin, M. Howell, G. Kassiotis, V. Libri, B. Williams, C. Swanton, S. Gandhi, D.L. Bauer, Neutralising antibody activity against SARS-CoV-2 VOCs B. 1.617. 2 and B. 1.351 by BNT162b2 vaccination, Lancet 397 (2021) 2331–2333.
[5] P. Mlcochova, S.A. Kemp, M.S. Dhar, G. Papa, B. Meng, I.A.T.M. Ferreira, R. Datir, D.A. Collier, A. Albecka, S. Singh, R. Pandey, J. Brown J, J. Zhou, N. Goonawardane, S. Mishra, C. Whittaker, T. Mellan, R. Marwal, M. Datta, S. Sengupta, K. Ponnusamy, V.S. Radhakrishnan, A. Abdullahi, O. Charles, P. Chattopadhyay, P. Devi, D. Caputo, T. Peacock, C. Wattal, N. Goel, A. Satwik, R. Vaishya, M. Agarwal, Indian SARS-CoV-2 genomics consortium (INSACOG), genotype to phenotype Japan (G2P-Japan) consortium, CITIID-NIHR BioResource COVID-19 Collaboration, in: A. Mavousian, J.H. Lee, J. Bassi, C. Silacci-Fegni, C. Saliba, D. Pinto, T. Irie, I. Yoshida, W.L. Hamilton, K. Sato, S. Bhatt, S. Flaxman, L.C. James, D. Corti, L. Piccoli, W.S. Barclay, P. Rakshit, A. Agrawal, R.K. Gupta (Eds.), SARS-CoV-2 B. 1. 617. 2 Delta Var. Replica Immune Evas., Nat. 599 (2021) 114–119.
[6] S. Xia, L. Wang, Y. Zhu, L. Lu, S. Jiang, Origin, virological features, immune evasion and intervention of SARS-CoV-2 Omicron sublineages, Sig. Transduct, Target Ther. 7 (2022) 241.
[7] M. McCallum, N. Czudnochowski, L.E. Rosen, S.K. Zepeda, J.E. Bowen, A.C. Walls, K. Hauser, A. Joshi, C. Stewart, J.R. Dillen, A.E. Powell, T.I. Croll, J. Nix, H.W. Virgin, D. Corti, G. Snell, D. Veesler, Structural basis of SARS-CoV-2 Omicron immune evasion and receptor engagement, Science 375 (2022) 864–868.
[8] R.H. Shaw, A. Stuart, M. Greenland, X. Liu, J.S. Nguyen Van-Tam, M.D. Snape, Com-COV Study Group, Heterologous prime-boost COVID-19 vaccination: initial reactogenicity data, Lancet 397 (2021) 2043–2046.
[9] N.C. Chiu, H. Chi, Y.K. Tu, Y.N. Huang, Y.L. Tai, S.L. Weng, L. Chang, D.T. Huang, F.Y. Huang, C.Y. Lin, To mix or not to mix? A rapid systematic review of heterologous prime-boost covid-19 vaccination, Expert Rev. Vaccin. 20 (2021) 1211–1220.
[10] R.L. Atmar, K.E. Lyke, M.E. Deming, L.A. Jackson, A.R. Branche, H.M. El Sahly, C.A. Rostad, J.M. Martin, C. Johnston, R.E. Rupp, M.J. Mulligan, R.C. Brady, R.W. Frenck Jr, M. Bäcker, A.C. Kottkamp, T.M. Babu, K. Rajakumar, S. Edupuganti, D. Dobrzynski, R.N. Coler, C.M. Posavad, J.I. Archer, S. Crandon, S.U. Nayak, D. Szydlo, J.A. Zemanek, C.P. Dominguez Islas, E.R. Brown, M.S. Suthar, M.J. McElrath, A.B. McDermott, S.E. O'Connell, D.C. Montefiori, A. Eaton, K.M. Neuzil, D.S. Stephens, P.C. Roberts, J.H. Beigel, DMID 21-0012 Study Group, Homologous and heterologous Covid-19 booster vaccinations, N. Engl. J. Med 386 (2022) 1046–1057.
[11] P.G. Kremsner, R.A. Ahuad Guerrero, E. Arana-Arri, G.J. Aroca Martinez, M. Bonten, R. Chandler, G. Corral, E.J.L. De Block, L. Ecker, J.J. Gabor, C.A. Garcia Lopez, L. Gonzales, M.A. Granados González, N. Gorini, M.P. Grobusch, A.D. Hrabar, H. Junker, A. Kimura, C.F. Lanata, C. Lehmann, I. Leroux-Roels, P. Mann, M.F. Martinez-Reséndez, T.J. Ochoa, C.A. Poy, M.J. Reyes Fentanes, L.M. Rivera Mejia, V.V. Ruiz Herrera, X. Sáez-Llorens, O. Schönborn-Kellenberger, M. Schunk, A. Sierra Garcia, I. Vergara, T. Verstraeten, M. Vico, L. Oostvogels, HERALD Study Group, Efficacy and safety of the CVnCoV SARS-CoV-2 mRNA vaccine candidate in ten countries in Europe and Latin America (HERALD): a randomised, observer-blinded, placebo-controlled, phase 2b/3 trial, Lancet Infect. Dis. 22 (2022) 329–340.
[12] S. Caillard, O. Thaunat, COVID-19 vaccination in kidney transplant recipients, Nat. Rev. Nephrol. 17 (2021) 785–787.
[13] E.J. Anderson, N.G. Rouphael, A.T. Widge, L.A. Jackson, P.C. Roberts, M. Makhene, J.D. Chappell, M.R. Denison, L.J. Stevens, A.J. Pruijssers, A.B. McDermott, B. Flach, B.C. Lin, N.A. Doria-Rose, S. O'Dell, S.D. Schmidt, K.S. Corbett, P.A. Swanson 2nd, M. Padilla, K.M. Neuzil, H. Bennett, B. Leav, M. Makowski, J. Albert, K. Cross, V.V. Edara, K. Floyd, M.S. Suthar, D.R. Martinez, R. Baric, W. Buchanan, C.J. Luke, V.K. Phadke, C.A. Rostad, J.E. Ledgerwood, B.S. Graham, J.H. Beigel, mRNA-1273 Study Group, Safety and immunogenicity of SARS-CoV-2 mRNA-1273 vaccine in older adults, N. Engl. J. Med. 383 (2020) 2427–2438.
[14] A.M. Hause, D.K. Shay, N.P. Klein, W.E. Abara, J. Baggs, M.M. Cortese, B. Fireman, J. Gee, J.M. Glanz, K. Goddard, K.E. Hanson, B. Hugueley, T. Kenigsberg, E.O. Kharbanda, B. Lewin, N. Lewis, P. Marquez, T. Myers, A. Naleway, J.C. Nelson, J.R. Su, D. Thompson, B. Olubajo, M.E. Oster, E.S. Weintraub, J.T.B. Williams, A.R. Yousaf, O. Zerbo, B. Zhang, T.,T. Shimabukuro, Safety of COVID-19 vaccination in United States children ages 5 to 11 years, Pediatrics 150 (2022) 2.
[15] D.A. Salmon, M.Z. Dudley, J.M. Glanz, S.B. Omer, Vaccine hesitancy: causes, consequences, and a call to action, Vaccine 33 (2015) D66–D71.
[16] A.D. Ravi, D. Sadhna, D. Nagpaal, L. Chawla, Needle free injection technology: a complete insight, Int. J. Pharm. Investig. 5 (2015) 192–199.
[17] S. Hu, Z. Li, J. Cores, K. Huang, T. Su, P.U. Dinh, K. Cheng, Needle-free injection of exosomes derived from human dermal fibroblast spheroids ameliorates skin photoaging, ACS Nano 13 (2019) 11273–11282.
[18] G. Egawa, K. Kabashima, Skin as a peripheral lymphoid organ: revisiting the concept of skin-associated lymphoid tissues, J. Invest. Dermatol. 131 (2011) 2178–2185.
[19] R.J. Hewitt, C.M. Lloyd, Regulation of immune responses by the airway epithelial cell landscape, Nat. Rev. Immunol. 21 (2021) 347–362.
[20] E.L. Giudice, J.D. Campbell, Needle-free vaccine delivery, Adv. Drug Deliv. Rev. 58 (2006) 68–89.
[21] J. Hu, H. Shi, C. Zhao, X. Li, Y. Wang, Q. Cheng, R. Goswami, Q. Zhen, M. Mei, Y. Song, S. Yang, Q. Li, Lispro administered by the QS-M Needle-Free Jet Injector generates an earlier insulin exposure, Expert Opin. Drug Deliv. 13 (2016) 1203–1207.
[22] T.R. Kwon, J. Seok, J.H. Jang, M.K. Kwon, C.T. Oh, E.J. Choi, H.K. Hong, Y.S. Choi, J. Bae, B.J. Kim, Needle-free jet injection of hyaluronic acid improves skin remodeling in a mouse model, Eur. J. Pharm. Biopharm. 105 (2016) 69–74.
[23] M.T. Yousafzai, A.F. Saleem, O. Mach, A. Baig, R.W. Sutter, A.K.M. Zaidi, Feasibility of conducting intradermal vaccination campaign with inactivated poliovirus vaccine using Tropis intradermal needle free injection system, Karachi, Pakistan, Heliyon 3 (2017) e00395.
[24] J.P. Amorij, W.L. Hinrichs, H.W. Frijlink, J.C. Wilschut, A. Huckriede, Needle-free influenza vaccination, Lancet Infect. Dis. 10 (2010) 699–711.
[25] F. Lebre, G. Borchard, M.C. de Lima, O. Borges, Progress towards a needle-free hepatitis B vaccine, Pharm. Res 28 (2011) 986–1012.
[26] E.A. Nelson, H.S. Lam, K.C. Choi, W.C. Ho, L.W. Fung, F.W. Cheng, R.Y. Sung, M. Royals, P.K. Chan, A pilot randomized study to assess immunogenicity, reactogenicity, safety and tolerability of two human papillomavirus vaccines administered intramuscularly and intradermally to females aged 18-26 years, Vaccine 31 (2013) 3452–3460.
[27] M. Isaka, T. Komiya, M. Takahashi, Y. Yasuda, T. Taniguchi, Y. Zhao, K. Matano, H. Matsui, J. Maeyama, K. Morokuma, K. Ohkuma, N. Goto, K. Tochikubo, Recombinant cholera toxin B subunit (rCTB) as a mucosal adjuvant enhances induction of diphtheria and tetanus antitoxin antibodies in mice by intranasal administration with diphtheria-pertussis-tetanus (DPT) combination vaccine, Vaccine 22 (2004) 3061–3068.
[28] C.H. Choi, C.A. Alabi, P. Webster, M.E. Davis, Mechanism of active targeting in solid tumors with transferrin-containing gold nanoparticles, Proc. Natl. Acad. Sci. U. S. A. 107 (2010) 235–240.
[29] A.V. Nguyen, A.M. Soulika, The dynamics of the Skin's immune system, Int. J. Mol. Sci. 20 (2019) 1811.
[30] J. Chen, R. Wang, M. Wang, G.W. Wei, Mutations strengthened SARS-CoV-2 infectivity, J. Mol. Biol. 432 (2020) 5212–5226.
[31] D. Zhou, W. Dejnirattisai, P. Supasa, C. Liu, A.J. Mentzer, H.M. Ginn, Y. Zhao, H.M.E. Duyvesteyn, A. Tuekprakhon, R. Nutalai, B. Wang, G.C. Paesen, C. Lopez-Camacho, J. Slon-Campos, B. Hallis, N. Coombes, K. Bewley, S. Charlton, T.S. Walter, D. Skelly, S.F. Lumley, C. Dold, R. Levin, T. Dong, A.J. Pollard, J.C. Knight, D. Crook, T. Lambe, E. Clutterbuck, S. Bibi, A. Flaxman, M. Bittaye, S. Belij-Rammerstorfer, S. Gilbert, W. James, M.W. Carroll, P. Klenerman, E. Barnes, S.J. Dunachie, E.E. Fry, J. Mongkolsapaya, J. Ren, D.I. Stuart, G.R. Screaton, Evidence of escape of SARS-CoV-2 variant B.1.351 from natural and vaccine-induced sera, Cell 184 (2021) 2348–2361.
[32] Y. Cao, J. Wang, F. Jian, T. Xiao, W. Song, A. Yisimayi, W. Huang, Q. Li, P. Wang, R. An, J. Wang, Y. Wang, X. Niu, S. Yang, H. Liang, H. Sun, T. Li, Y. Yu, Q. Cui, S. Liu, X. Yang, S. Du, Z. Zhang, X. Hao, F. Shao, R. Jin, X. Wang, J. Xiao, Y. Wang, X.S. Xie, Omicron escapes the majority of existing SARS-CoV-2 neutralizing antibodies, Nature 602 (2022) 657–663.
[33] S. Kumar, K. Karuppanan, G. Subramaniam, Omicron (BA.1) and sub-variants (BA.1.1, BA.2, and BA.3) of SARS-CoV-2 spike infectivity and pathogenicity: A comparative sequence and structural-based computational assessment, J. Med. Virol. 94 (2022) 4780–4791.
[34] B.A. Johnson, X. Xie, A.L. Bailey, B. Kalveram, K.G. Lokugamage, A. Muruato, J. Zou, X. Zhang, T. Juelich, J.K. Smith, L. Zhang, N. Bopp, C. Schindewolf, M. Vu, A. Vanderheiden, E.S. Winkler, D. Swetnam, J.A. Plante, P. Aguilar, K.S. Plante, V. Popov, B. Lee, S.C. Weaver, M.S. Suthar, A.L. Routh, P. Ren, Z. Ku, Z. An, K. Debbink, M.S. Diamond, P.Y. Shi, A.N. Freiberg, V.D. Menachery, Loss of furin cleavage site attenuates SARS-CoV-2 pathogenesis, Nature 591 (2021) 293–299.
[35] C.L. Hsieh, J.A. Goldsmith, J.M. Schaub, A.M. DiVenere, H.C. Kuo, K. Javanmardi, K.C. Le, D. Wrapp, A.G. Lee, Y. Liu, C.W. Chou, P.O. Byrne, C.K. Hjorth, N.V. Johnson, J. Ludes-Meyers, A.W. Nguyen, J. Park, N. Wang, D. Amengor, J.J. Lavinder, G.C. Ippolito, J.A. Maynard, I.J. Finkelstein, J.S. McLellan, Structure-based design of prefusion-stabilized SARS-CoV-2 spikes, Science 369 (2020) 1501–1505.
[36] Y. Yuan, D. Cao, Y. Zhang, J. Ma, J. Qi, Q. Wang, G. Lu, Y. Wu, J. Yan, Y. Shi, X. Zhang, G.F. Gao, Cryo-EM structures of MERS-CoV and SARS-CoV spike glycoproteins reveal the dynamic receptor binding domains, Nat. Commun. 8 (2017) 15092.
[37] A. Khurana, P. Allawadhi, I. Khurana, S. Allwadhi, R. Weiskirchen, A.K. Banothu, D. Chhabra, K. Joshi, K.K. Bharani, Role of nanotechnology behind the success of mRNA vaccines for COVID-19, Nano Today 38 (2021) 101142, https://doi.org/10.1016/j.nantod.2021.101142
[38] M. Papi, D. Pozzi, V. Palmieri, G. Caracciolo, Principles for optimization and validation of mRNA lipid nanoparticle vaccines against COVID-19 using 3D bioprinting, Nano Today 43 (2022) 101403, https://doi.org/10.1016/j.nantod.2022.101403
[39] X. Hou, T. Zaks, R. Langer, Y. Dong, Lipid nanoparticles for mRNA delivery, Nat. Rev. Mater. 6 (2021) 1078–1094.
[40] T.E. Tallei, S. Alhumaid, Z. AlMusa, D.Kusumawaty Fatimawali, A. Alynbiawi, A.N. Alshukairi, A.A. Rabaan, Update on the omicron sub-variants BA.4 and BA.5, Rev. Med Virol.. 26 (2022) e2391.
[41] W. Ni, X. Yang, D. Yang, J. Bao, R. Li, Y. Xiao, C. Hou, H. Wang, J. Liu, D. Yang, Y. Xu, Z. Cao, Z. Gao, Role of angiotensin-converting enzyme 2 (ACE2) in COVID-19, Crit. Care 24 (2022) 422.
[42] H. Cheng, Y. Wang, G.Q. Wang, Organ-protective effect of angiotensin-converting enzyme 2 and its effect on the prognosis of COVID-19, J. Med. Virol. 92 (2020) 726–730.
[43] A.R. Bourgonje, A.E. Abdulle, W. Timens, J.L. Hillebrands, G.J. Navis, S.J. Gordijn, M.C. Bolling, G. Dijkstra, A.A. Voors, A.D. Osterhaus, P.H. van der Voort, D.J. Mulder, H. van Goor, Angiotensin-converting enzyme 2 (ACE2), SARS-CoV-2

and the pathophysiology of coronavirus disease 2019 (COVID-19), J. Pathol. 251 (2020) 228–248.
[44] I. Chakraborty, P. Maity, COVID-19 outbreak: migration, effects on society, global environment and prevention, Sci. Total Environ. 728 (2020) 138882.
[45] N. Donthu, A. Gustafsson, Effects of COVID-19 on business and research, J. Bus. Res 117 (2020) 284–289.
[46] E. Miguel, A.M. Mobarak, The economics of the COVID-19 pandemic in poor countries, Annu. Rev. Econom. 14 (2022) 253–285.
[47] D. Mostaghimi, C.N. Valdez, H.T. Larson, C.C. Kalinich, A. Iwasaki, Prevention of host-to-host transmission by SARS-CoV-2 vaccines, Lancet Infect. Dis. 22 (2022) e52–e58.
[48] D. Ndwandwe, C.S. Wiysonge, COVID-19 vaccines, Curr. Opin. Immunol. 71 (2021) 111–116.
[49] W.T. Harvey, A.M. Carabelli, B. Jackson, R.K. Gupta, E.C. Thomson, E.M. Harrison, C. Ludden, R. Reeve, A. Rambaut, COVID-19 Genomics UK (COG-UK) Consortium, S.J. Peacock, D.L. Robertson, SARS-CoV-2 variants, spike mutations and immune escape, Nat. Rev. Microbiol. 19 (2021) 409–424.
[50] P.V. Markov, A. Katzourakis, N.I. Stilianakis, Antigenic evolution will lead to new SARS-CoV-2 variants with unpredictable severity, Nat., Rev. Microbiol. 20 (2022) 251–252.
[51] F. Zuo, H. Abolhassani, L. Du, A. Piralla, F. Bertoglio, L. de Campos-Mata, H. Wan, M. Schubert, I. Cassaniti, Y. Wang, J.C. Sammartino, R. Sun, S. Vlachiotis, F. Bergami, M. Kumagai-Braesch, J. Andréll, Z. Zhang, Y. Xue, E.V. Wenzel, L. Calzolai, L. Varani, N. Rezaei, Z. Chavoshzadeh, F. Baldanti, M. Hust, L. Hammarström, H. Marcotte, Q. Pan-Hammarström, Heterologous vaccination with inactivated vaccine followed by mRNA-booster elicits strong immunity against SARS-CoV-2 Omicron variant, Nat. Commun. 13 (2022) 2670.
[52] X. Wang, X. Zhao, J. Song, J. Wu, Y. Zhu, M. Li, Y. Cui, Y. Chen, L. Yang, J. Liu, H. Zhu, S. Jiang, P. Wang, Homologous or heterologous booster of inactivated vaccine reduces SARS-CoV-2 Omicron variant escape from neutralizing antibodies, Emerg. Microbes Infect. 11 (2022) 477–481.
[53] E. Pérez-Then, C. Lucas, V.S. Monteiro, M. Miric, V. Brache, L. Cochon, C.B.F. Vogels, A.A. Malik, E. De la Cruz, A. Jorge, M. De Los Santos, P. Leon, M.I. Breban, K. Billig, I. Yildirim, C. Pearson, R. Downing, E. Gagnon, A. Muyombwe, J. Razeq, M. Campbell, A.I. Ko, S.B. Omer, N.D. Grubaugh, S.H. Vermund, A. Iwasaki, Neutralizing antibodies against the SARS-CoV-2 Delta and Omicron variants following heterologous CoronaVac plus BNT162b2 booster vaccination, Nat. Med. 28 (2022) 481–485.
[54] S.M.S. Cheng, C.K.P. Mok, Y.W.Y. Leung, S.S. Ng, K.C.K. Chan, F.W. Ko, C. Chen, K. Yiu, B.H.S. Lam, E.H.Y. Lau, K.K.P. Chan, L.L.H. Luk, J.K.C. Li, L.C.H. Tsang, L.L.M. Poon, D.S.C. Hui, M. Peiris, Neutralizing antibodies against the SARS-CoV-2 Omicron variant BA.1 following homologous and heterologous CoronaVac or BNT162b2 vaccination, Nat. Med. 28 (2022) 486–489.
[55] X. Kong, M. Luo, L. Cai, P. Zhang, R. Yan, Y. Hu, H. Li, J. Ma, Needle-free jet injection of insulin glargine improves glycemic control in patients with type 2 diabetes mellitus: a study based on the flash glucose monitoring system, Expert Opin. Drug Deliv. 18 (2021) 635–641.
[56] R. Verbeke, I. Lentacker, S.C.D. Smedt, H. Dewitte, Three decades of messenger RNA vaccine development, Nano Today 28 (2019) 100766, https://doi.org/10.1016/j.nantod.2019.100766
[57] S. Franzé, F. Selmin, E. Samaritani, P. Minghetti, Cilurzo F Lyophilization of liposomal formulations: still necessary, still challenging, Pharmaceutics 10 (2018) E139.
[58] M. Mohammady, Y. Mohammadi, G. Yousefi, Freeze-Drying of pharmaceutical and nutraceutical nanoparticles: the effects of formulation and technique parameters on nanoparticles characteristics, J. Pharm. Sci. 109 (2020) 3235–3247.

Dr. Mao Shanhong currently is a professor and Ph.D supervisor at Biomedical Engineering School of Chinese Capital Medical University. He also serves as Chief Counsellor and Visiting Fellow of Chinese Academy of Inspection and Quarantine Sciences. Dr. Mao has more than 30 years of experiences in healthcare innovation, with expertise in pharmaceuticals, medical devices, AI, and material science. He holds more than 20 patents and over 40 peer-reviewed publications. Dr. Mao received his EMBA from Carlson School of Business at University of Minnesota, PhD from UC Berkeley, MSc from Tsinghua University and BA from Peking University.

Dr. Li is the co-founder and CTO (Chief Technology Officer) of tricisionbio Therapeutics, Inc. He has over 10 years of research experience at the Beijing Institute of Genome (BIG) , Chinese Academy of Sciences (CAS). He also served as a senior scientist and director of R&D at HDBiosciences / WuXi AppTec for over 10 years. Dr. Li received his PhD training program at the Beijing Genomics Institute. Currently, his team in tricisionbio is focused on the pre-clinical and clinical development of novel vaccine approaches and therapeutic technologies for cancer and infectious diseases.

Mr. Zhang Yuxin is the founder and CEO of Beijing QS Medical Technology Co. Ltd.(Quinovare). He graduated from Conservatoire National Des Arts et Métiers (CNAM) with a master degree. He established the Needle-free Injection Technology Research Center in 2005 and founded the Quinovare in 2007. Mr. Zhang led Quinovare to draft the Chinese industry standard of needle-free injection, assist domestic well-known nursing experts to develop the world's first needle-free injection operation guide, as well as assist domestic authoritative endocrinologists to incorporate needle-free medicine delivery technology into the diabetes treatment guide.